Karlsruhe Institute of Technology

Fakultät für Physik
Institut für Theorie der Kondensierten Materie

Another thesis on SNS junctions: numerical simulations and calculations

Master's Thesis

by

Umut Nefta Kanilmaz

Submission date: 25. February 2018

Advisor: PD Dr. Igor Gornyi
Co-Advisor: Prof. Dr. Alexander Mirlin

Ich erkläre hiermit, dass die Arbeit selbstständig angefertigt, alle benutzten Quellen und Hilfsmittel vollständig und genau angegeben und alles kenntlich gemacht wurde, das aus Arbeiten anderer unverändert oder mit Abänderungen entnommen ist.

Karlsruhe, den 23. Februar 2018

Umut Nefta Kanilmaz

Contents

1 Experimental set-up

2 Framework for analytical model

2.1 Theory of superconductivity

The discovery of the isotope effect in 1950 revealed that not only lattice electrons but rather the whole lattice determines the superconducting properties of a solid. Experiments measuring the critical temperature T_c of different mercury isotopes showed that indeed, there is a relation between the isotope mass and T_c. Herbert Frölich was then the first to introduce a new concept to explain superconductivity. He showed that a phonon-intermediated interaction between electrons and the lattice could lead to an attractive long-range interaction of electrons in the lattice. Figuratively speaking, an electron passing through the crystal lattice will polarize it by attracting the positive ions. It leaves a deformed lattice, which will then attract a second electron. An effective attractive interaction between these two electrons is created. In 1956, Cooper showed that the electronic ground state, the Fermi sea at $T = 0$, is unstable if a weak attractive interaction is taken into account. This layed the foundation of the BCS theory [1], the first microscopic theory after the discovery in 1911 by Heike Kammerlingh Onnes.

Formulas needed

Hamiltonian:

$$H = H_0 + H_1 \tag{2.1}$$

$$H_0 = \sum_{\mathbf{k},\sigma} \xi_{\mathbf{k}} c^\dagger_{\mathbf{k}\sigma} c_{\mathbf{k}\sigma} \tag{2.2}$$

$$H_1 = \frac{1}{N} \sum_{\mathbf{k},\mathbf{k}'} V_{\mathbf{k},\mathbf{k}'} c^\dagger_{\mathbf{k}\uparrow} c^\dagger_{-\mathbf{k}\downarrow} c_{-\mathbf{k}'\downarrow} c_{\mathbf{k}'\uparrow} \tag{2.3}$$

The operators $c^\dagger_{\mathbf{k},\sigma}, c_{\mathbf{k},\sigma}$ are fermion operators that create or annihilate an electron with momentum $\mathbf{k}$ and spin σ. The first term in the Hamiltonian H is the unperturbed electron Hamiltonian H_0 with parabolic energy dispersion $\xi_{\mathbf{k}}$. The second term is the interaction Hamiltonian H_1, expressing the scattering of two electrons from $(-\mathbf{k}' \downarrow, \mathbf{k}' \uparrow)$ to $(\mathbf{k} \uparrow, -\mathbf{k} \downarrow)$. The interaction potential $V_{\mathbf{k},\mathbf{k}'}$ exchanges the scattering for electrons with energy $|\xi_{\mathbf{k}}| \lesssim \hbar\omega_D$. The Hamiltonian in eq. (2.1) can be simplified by doing a mean-field approximation. In this approximation, an operator A is expressed by a sum of its statistical mean $\langle A \rangle$ and small statistical fluctuations δA. Since the fluctuations

are assumed to be small, terms with $\mathcal{O}((\delta A)^2)$ can be neglected.

$$\begin{aligned} A &= \langle A\rangle + \delta A, \quad B = \langle B\rangle + \delta B \\ AB &= \langle A\rangle\langle B\rangle + \langle A\rangle\delta B + \langle B\rangle\delta A + \underbrace{\delta A\delta B}_{\approx 0} \end{aligned} \tag{2.4}$$

Using $\delta A = A - \langle A\rangle$ and inserting this back into eq. (2.4) leads to

$$AB = \langle A\rangle B + \langle B\rangle A - \langle A\rangle\langle B\rangle. \tag{2.5}$$

This approximation is applied to the interaction part H_1 in eq. (2.3), replacing

$$A = c^\dagger_{\mathbf{k}\uparrow}c^\dagger_{-\mathbf{k}\downarrow}, \quad B = c_{-\mathbf{k}'\downarrow}c_{\mathbf{k}'\uparrow}. \tag{2.6}$$

The result is the BCS-Hamiltonian

$$H_{\mathrm{BCS}} = \sum_{\mathbf{k},\sigma}\xi_{\mathbf{k}}c^\dagger_{\mathbf{k}\sigma}c_{\mathbf{k}\sigma} - \sum_{\mathbf{k}}\Delta^*_{\mathbf{k}}c_{-\mathbf{k},\downarrow}c_{\mathbf{k},\uparrow} - \sum_{\mathbf{k}}\Delta_{\mathbf{k}}c^\dagger_{\mathbf{k}\uparrow}c^\dagger_{-\mathbf{k}\downarrow} + \text{const.} \tag{2.7}$$

where

$$\Delta_{\mathbf{k}} := -\frac{1}{N}\sum_{\mathbf{k}'}V_{\mathbf{k}\mathbf{k}'}\langle c_{-\mathbf{k}',\downarrow}c_{\mathbf{k}'\uparrow}\rangle \tag{2.8}$$

$$\Delta^*_{\mathbf{k}} := -\frac{1}{N}\sum_{\mathbf{k}'}V_{\mathbf{k},\mathbf{k}'}\langle c^\dagger_{\mathbf{k}'\uparrow}c^\dagger_{-\mathbf{k}'\downarrow}\rangle \tag{2.9}$$

The BCS-Hamiltonian in eq. (2.7) can be diagonalized using the Bogoliubov transformation. The aim is to express the Hamiltonian in the basis of new fermion operators. These new operators will describe quasiparticles, which are a linear combination of $c^\dagger_{\mathbf{k},\sigma}$ and $c_{\mathbf{k},\sigma}$.

$$\begin{pmatrix}\gamma_{\mathbf{k}\uparrow}\\ \gamma^\dagger_{-\mathbf{k}\downarrow}\end{pmatrix} = \begin{pmatrix}u^*_{\mathbf{k}} & -v_{\mathbf{k}}\\ v^*_{\mathbf{k}} & u_{\mathbf{k}}\end{pmatrix}\begin{pmatrix}c_{\mathbf{k}\uparrow}\\ c^\dagger_{-\mathbf{k}\downarrow}\end{pmatrix} \tag{2.10}$$

Evaluating the fermion anticommutation relation using the transformation above yields

$$\left\{\gamma_{\mathbf{k}\uparrow}, \gamma^\dagger_{\mathbf{k}\uparrow}\right\} = \cdots = |u_{\mathbf{k}}|^2| + v_{\mathbf{k}}|^2 \stackrel{!}{=} 1 \tag{2.11}$$

and will lead to the inverse transformation of eq. (2.1). Inserting the inverse transformation into the BCS-Hamiltonian in eq.(2.7) will give the coefficients $u_{\mathbf{k}}$, $v_{\mathbf{k}}$ from eq. (2.1) and finally yield to the diagonalized form of the BCS-Hamiltonian

$$H_{\mathrm{BCS}} = \sum_{\mathbf{k}\sigma}E_{\mathbf{k}}\gamma^\dagger_{\mathbf{k}\sigma}\gamma_{\mathbf{k}\sigma} \tag{2.12}$$

$$E_{\mathbf{k}} := \sqrt{\xi^2_{\mathbf{k}} + |\Delta_{\mathbf{k}}|^2} \tag{2.13}$$

For a fixed energy E_k, eq. (2.13) gives two possible values for ξ_k:

$$\xi_k = \pm\sqrt{\epsilon^2 - |\Delta_k|^2}. \tag{2.14}$$

Knowing that $k^2 = k_F^2 \pm 2m\sqrt{\epsilon^2 + |Delta_k|^2}\hbar^2$, one can calculate the group velocity as

$$v_g = \frac{d\epsilon}{d(\hbar k)} = \pm v_F\frac{\sqrt{\epsilon^2 - |\Delta|^2}}{\epsilon}. \tag{2.15}$$

The group velocity is positive for excitations outside the Fermi surface and negative for excitations inside. Therefore, the positive solution is a particle-like excitation, and the negative solution is a hole-like excitation. Figure 2.1 shows the excitation spectrum of particles and holes from the BCS theory.

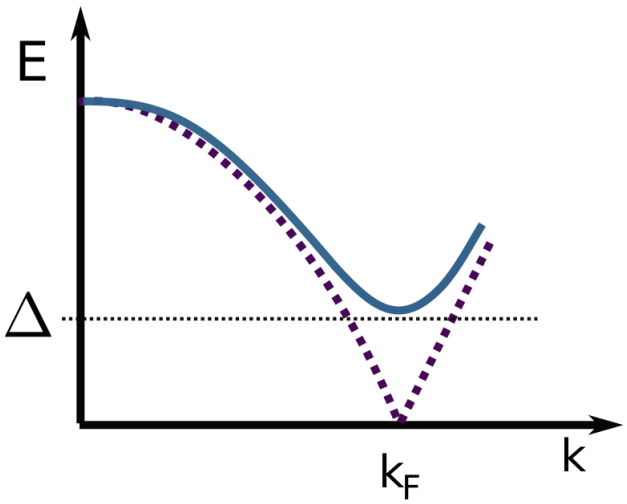

Figure 2.1: *Excitations from BCS theory. The dashed line is the normal state dispersion relation ($\Delta = 0$). The solid line is the dispersion relation for the superconducting state ($\Delta \neq 0$), where no excitations with energies $\epsilon < \Delta$ are present.*

Bogoliubov de Gennes Hamiltonian

The ansatz for the BCS ground state used by Bardeen, Cooper and Schrieffer is based on the concept of Cooper pairs. It is a direct consequence of the instability in the ground state through the attractive interaction. The BCS theory proposes a BCS ground state built on eigenstates of the single-particle Hamiltonian H_0 from eq. (2.2), leading to a ground state that consists of a linear combination of pair states.

$$|\psi_{\mathrm{BCS}}\rangle = \prod_{\mathbf{k}} (u_{\mathbf{k}} + v_{\mathbf{k}} c^{\dagger}_{\mathbf{k}\uparrow} c^{\dagger}_{-\mathbf{k}\downarrow}) |\mathrm{vac}\rangle \tag{2.16}$$

$$H_{\mathrm{BCS}} |\psi_{\mathrm{BCS}}\rangle = E_{\mathrm{BCS}} |\psi_{\mathrm{BCS}}\rangle \tag{2.17}$$

In most cases however, a more realistic set-up or inhomogeneous system cannot be described in terms of eigenfunctions of H_0. With a vector potential $\mathbf{A} \neq 0$, for example, time reversal symmetry is not given any more. The characteristic length scale is the superconducting coherence length ξ_0. If a system is varying slowly over a length scale $l \approx \xi_0$, a spatially dependent, more general Hamiltonian is needed. In order to find an adequate expression for such a spatially dependent Hamiltonian, the following spinor is introduced

$$|\Psi_{\mathbf{k}}\rangle = \begin{pmatrix} |\Psi_{\mathbf{k_1}}\rangle \\ |\Psi_{\mathbf{k_2}}\rangle \end{pmatrix} := \begin{pmatrix} c^{\dagger}_{\mathbf{k},\uparrow} \\ c_{-\mathbf{k},\downarrow} \end{pmatrix} |\psi_{\mathrm{BCS}}\rangle \tag{2.18}$$

In this basis $\left\{ |\Psi_{\mathbf{k_1}}\rangle, |\Psi_{\mathbf{k_2}}\rangle \right\}$, the Hamiltonian is (and this is the Bogoliubov de Gennes Hamiltonian with energies relative to $E_{\mathbf{k}}$):

$$H_{\mathrm{BdG}}(\mathbf{k}) = \begin{pmatrix} \xi_{\mathbf{k}} & -\Delta_{\mathbf{k}} \\ -\Delta^{*}_{\mathbf{k}} & -\xi_{\mathbf{k}} \end{pmatrix} \tag{2.19}$$

This Hamiltonian form eq. (2.19) has the eigenvalues

$$\pm E_{\mathbf{k}} = \pm \sqrt{\xi^2_{\mathbf{k}} + |\Delta_{\mathbf{k}}|^2}. \tag{2.20}$$

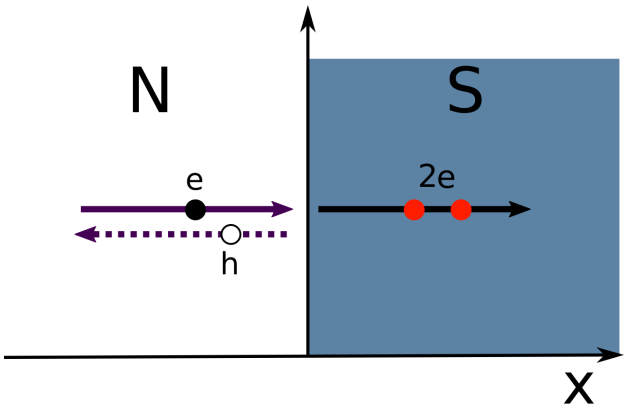

Figure 2.2: *Andreev reflection at an NS interface. An incoming electron is Andreev reflected into a hole with opposite momentum, and a Cooper pair condensates into the superconductor. The interface is modelled as a sharp edge.*

To finally arrive at the spatially dependent form of eg. (2.19), the Hamiltonian is Fourier-transformed.

$$H_{\mathrm{BdG}}(\mathbf{r}) := \frac{1}{N}\sum_{\mathbf{k}} e^{i\mathbf{k}\cdot\mathbf{r}} H_{\mathrm{BdG}}(\mathbf{k}) \tag{2.21}$$

$$= \begin{pmatrix} H_0(\mathbf{r}) & -\Delta(\mathbf{r}) \\ -\Delta^*(\mathbf{r}) & -H_0(\mathbf{r}) \end{pmatrix} \tag{2.22}$$

$H_0(\mathbf{r})$ is the free Hamiltonian. Corresponding Schrödinger equaions are called BdG-equations:

$$H_{\mathrm{BdG}}(\mathbf{r})\,\Psi(\mathbf{r}) = E\Psi(\mathbf{r}) \tag{2.23}$$

$$\Psi(\mathbf{r}) = \begin{pmatrix} \Psi_1(\mathbf{r}) \\ \Psi_2(\mathbf{r}) \end{pmatrix} \tag{2.24}$$

2.2 Andreev reflection- NS interface

Now that the principles of BCS theory have been established, the physical effects at the interface between a superconductor and a normal are to be outlined.
The most important detail when modelling the interface between a superconductor and a normal metal is the superconducting order parameter $\Delta(\mathbf{r})$. It is present in the superconducting region and zero in a normal metal. To keep the model as simple as possible, a step-like behaviour is assumed. This means that for an interface placed at $x = 0$, the superconducting order parameter becomes a function of x and can be written as

$$\Delta(x) = \theta(x)\,. \tag{2.25}$$

How does this model differ from a quantum mechanical step potential set-up? The formalism is virtually identical, but there is a subtle and important difference in the results. In the normal region, there are electrons, whereas in the superconducting regions, there is a condensate of Cooper pairs. A normal electron can be reflected at the interface as a hole and an additional Cooper pair can be created in the superconducting region (see figure 2.2). By solving the Bogoliubov-de-Gennes equation in (2.23), this picture becomes clearer. This equation needs to be solved

both for the normal and the superconducting region. When treating this problem quantum-mechanically, energies below and above the gap need to be considered independently. The resulting wave functions have to be continuous at the interface. Depending on the region, the gap parameter in the Hamiltonian in eq. (2.22) is either zero or Δ_0.

Semi-classical approximation: Andreev equations

In case of the NS interface, the gap parameter varies slowly over scales of k_F, and it may vary over scales of the coherence length ξ_0. Because k_F is a good length scale for this problem, the equations above can be simplified:

$$\Psi(\mathbf{r}) = e^{i\mathbf{k_F}\mathbf{r}} \begin{pmatrix} u(\mathbf{r}) \\ v(\mathbf{r}) \end{pmatrix}. \tag{2.26}$$

Since $u(\mathbf{r})$ and $v(\mathbf{r})$ vary slowly over distances of order k_F^{-1}, the second derivative can be neglected. This is the semi-classical approximation, which then leads to the Andreev equations

$$-i\hbar \mathbf{v}_F \nabla u(\mathbf{r}) + \Delta(\mathbf{r}) v(\mathbf{r}) = \epsilon u(\mathbf{r}) \tag{2.27}$$

$$i\hbar \mathbf{v}_F \nabla v(\mathbf{r}) + \Delta^*(\mathbf{r}) u(\mathbf{r}) = \epsilon v(\mathbf{r}). \tag{2.28}$$

These equations are significantly easier to handle than the BdG-equations, since they describe a first-order problem.

Consider an incoming particle from the left half-space $x < 0$, travelling towards the superconducting interface at $x = 0$, assuming that both the normal region and the superconductor have the same Fermi velocity k_F^{-1}. The one-dimensional Andreev equations for the NS interface read

$$-i\hbar v_{F,x} \frac{d}{dx} u(x) + \Delta(x) v(x) = \epsilon u(x) \tag{2.29}$$

$$i\hbar v_{F,x} \frac{d}{dx} v(x) + \Delta^*(x) u(x) = \epsilon v(x). \tag{2.30}$$

In the normal region (for $x < 0$) the superconducting gap parameter decreases to zero on a length scale shorter than ξ. Therefore, the step-like approximation from eq. (2.25) holds. In the normal region, the coefficients $u(x)$ and $v(x)$ are independent. The ansatz contains an incident wave with unity amplitude and a reflected hole with amplitude r.

$$\Psi_N(x) = \begin{pmatrix} u(x) \\ v(x) \end{pmatrix}_N = e^{ik_N x} \begin{pmatrix} 1 \\ 0 \end{pmatrix} + r e^{-ik_N x} \begin{pmatrix} 0 \\ 1 \end{pmatrix} \tag{2.31}$$

where, writing $v_x \equiv v_{F,x}$,

$$k_N = \frac{\epsilon}{\hbar v_x} \tag{2.32}$$

In the superconducting region, the solution for the wave function has the form

$$\Psi_S(x) = \begin{pmatrix} u(x) \\ v(x) \end{pmatrix}_S = t e^{ik_S x} \begin{pmatrix} u_0 \\ v_0 \end{pmatrix}. \tag{2.33}$$

The expression for the wave vector k_S depends on the energy of the incoming particle, which can be either *above* or *below* the gap.

For high energies *above* the gap, $\epsilon > |\Delta|$, the wave vector is

$$k_S = \frac{\sqrt{\epsilon^2 - \Delta^2}}{\hbar v_x} \tag{2.34}$$

If the energy of the incoming particle is higher than the gap energy, it can be transmitted into the superconductor. The amplitude t therefore is the transmission probability. The coherence factors u_0, v_0 can be found by solving the BdG equations within the BCS framework. Matching the boundary conditions at the interface yields

$$r = \frac{v_0}{u_0}, \quad t = \frac{1}{u_0}. \tag{2.35}$$

Normalizing the wave functions leads to

$$|r|^2 + (u_0^2 - v_0^2)|t|^2 = 1 \tag{2.36}$$

Since ϵ is the energy relative to the Fermi energy, the normal wave vector from eq. (2.31) can be written in terms of

$$\mathbf{q}_\pm = \left(k_F \pm \frac{\epsilon}{\hbar v_F}\right) \hat{\mathbf{k}_F} \tag{2.37}$$

$$\Psi_N(\mathbf{r}) = e^{i\mathbf{q}_+ \cdot \mathbf{r}} \begin{pmatrix} 1 \\ 0 \end{pmatrix} + a e^{i\mathbf{q}_- \cdot \mathbf{r}} \begin{pmatrix} 0 \\ 1 \end{pmatrix}, \tag{2.38}$$

Using eq. (2.37), one finds the trajectory of the reflected hole to coincide with the trajectory of the incoming electron. The change in momentum,

$$\Delta p_x = -\frac{2e}{v_x}, \tag{2.39}$$

Δp_x is small. The components p_y, p_z are conserved, therefore the trajectory of the reflected hole is almost the same as the trajectory of the incoming electron.

For energies *below* the gap, $\epsilon < |\Delta|$, there are no states available inside the gap, therefore the wave function decays inside the superconductor.

$$\tilde{k}_S = \frac{\sqrt{\Delta^2 - \epsilon^2}}{\hbar v_x}. \tag{2.40}$$

The wave function is

$$\begin{pmatrix} u(x) \\ v(x) \end{pmatrix}_S = t e^{-\tilde{k_S} x} \begin{pmatrix} u_0 \\ v_0 \end{pmatrix}. \tag{2.41}$$

For sub-gap energies, the amplitudes of the normal wave functions are slightly modified:

$$r = \frac{\tilde{v_0}}{\tilde{u_0}}, \quad t = \frac{1}{\tilde{u_0}} \tag{2.42}$$

and

$$\tilde{u_0} = \frac{1}{\sqrt{2}} \left(1 + i\frac{\sqrt{|\Delta|^2 - \epsilon^2}}{\epsilon}\right), \quad \tilde{v_0} = \frac{1}{\sqrt{2}} \left(1 - i\frac{\sqrt{|\Delta|^2 - \epsilon^2}}{\epsilon}\right). \tag{2.43}$$

In this case, it holds that

$$|a|^2 = 1 \tag{2.44}$$

In other words, there are no transmitted particles and all particles are Andreev reflected.

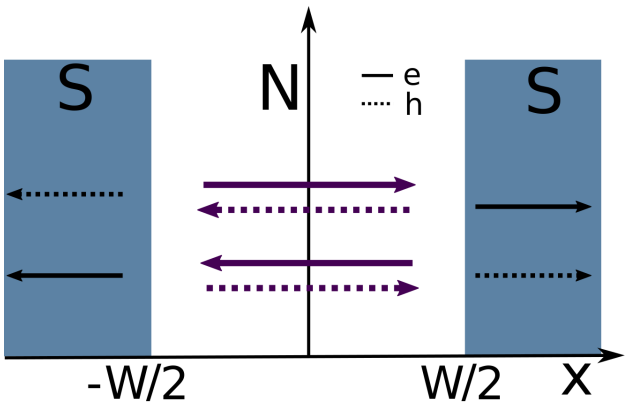

Figure 2.3: *A SNS junction with width W. Electrons are indicated as solid arrow, holes as dashed ones. An electron (hole) is Andreev reflected as a hole (electron) at one side, which then again is reflected at the other side. In this way, Andreev bound states form in the junction.*

2.3 Theory of SNS junction

So far, only NS interfaces have been considered. The same procedure can be applied to superconductor - normal metal - superconductor (SNS) junctions: A sandwich structure of a superconductor on the left side, a normal region in the middle and a superconductor on the right side. At both interfaces, a particle can be Andreev-reflected. Each time an electron is Andreev reflected at the right side and a hole travels back, a cooper pair is induced into the right superconductor. In the same manner, a cooper pair is stolen from the left superconductor when the hole is Andreev reflected as an electron. This process is illustrated in figure 2.3. As an overall consequence, a supercurrent through the SNS junction can be observed. This process leads to localized electrons with bound states, the so called Andreev bound states.

A SNS junction with normal region at $|x| < W/2$, the right superconductor at $x > +W/2$ and the left superconductor at $x < -W/2$ is considered. The electrons in both superconducting regions and in the normal metal have the same Fermi velocity and there are no insulating barriers between them. This means that W is smaller than the electron mean free path. For short W this implies that the mean free path is larger than the superconducting coherence length (?). The phase difference between the superconductors is χ, so the right supercondctor has phase $\chi/2$ and the left has $-\chi/2$. The semi classical approximation is used and a wave function with the form

$$\Psi(\mathbf{r}) = e^{i\mathbf{k_F}\mathbf{r}} \begin{pmatrix} u(\mathbf{r}) \\ v(\mathbf{r}) \end{pmatrix}. \tag{2.45}$$

is needed. In the normal region, it holds that

$$\Psi_N(x) = A \cdot \left[e^{ik_N x} \begin{pmatrix} 1 \\ 0 \end{pmatrix} + a e^{-ik_N x} \begin{pmatrix} 0 \\ 1 \end{pmatrix} \right], \tag{2.46}$$

$$k_N = \frac{\epsilon}{\hbar v_x}. \tag{2.47}$$

Assuming that $k_x > 0$, the wave function in the right superconductor ($x > W/2$) is

$$\Psi_S^R(x) = d_1 e^{-\tilde{k}_S x} \begin{pmatrix} \tilde{u}_0 e^{i\chi/4} \\ \tilde{v}_0 e^{-i\chi/4} \end{pmatrix}, \tag{2.48}$$

$$\tilde{k}_S = \frac{\sqrt{|\Delta|^2 - \epsilon^2}}{\hbar |v_x|}. \tag{2.49}$$

For the left superconductor, the wave function is

$$\Psi_S^L(x) = d_1' e^{\tilde{k}_S x} \begin{pmatrix} \tilde{v}_0 e^{-i\chi/4} \\ \tilde{u}_0 e^{i\chi/4} \end{pmatrix}. \tag{2.50}$$

Applying the continuity condition at the interfaces leads to

$$a e^{-ik_n W} = \frac{\tilde{v}_0}{\tilde{u}_0} e^{-i\chi/2} \tag{2.51}$$

$$a e^{ik_n W} = \frac{\tilde{u}_0}{\tilde{v}_0} e^{i\chi/2}. \tag{2.52}$$

Combining these equations, we find

$$e^{2i(k_N W - \chi/2)} = \frac{\epsilon + i\sqrt{|\Delta|^2 - \epsilon^2}}{\epsilon - i\sqrt{|\Delta|^2 - \epsilon^2}}. \tag{2.53}$$

To simplify this expression, one can introduce

$$\sin\alpha := \frac{\epsilon}{|\Delta|}, \quad -\pi/2 < \alpha < \pi/2 \tag{2.54}$$

Using eq. (2.54), one can rewrite the right hand side of eq. (2.53) in terms of trigonometric functions and gets

$$e^{2i(k_N W - \chi/2)} = e^{-2i\alpha + i\pi}, \tag{2.55}$$

which then leads to

$$\epsilon = \frac{\hbar v_x}{W}\left(\pi\left(l + \frac{1}{2}\right) - \arcsin\frac{\epsilon}{|\Delta|} + \frac{\chi}{2}\right). \tag{2.56}$$

If $k_x < 0$, it holds that

$$\Psi_S^R(x) = d_2 e^{-\tilde{k}_S x} \begin{pmatrix} \tilde{v}_0 e^{i\chi/4} \\ \tilde{u}_0 e^{-i\chi/4} \end{pmatrix} \tag{2.57}$$

For the left superconductor, the wave function is

$$\Psi_S^L(x) = d_2' e^{\tilde{k}_S x} \begin{pmatrix} \tilde{u}_0 e^{-i\chi/4} \\ \tilde{v}_0 e^{i\chi/4} \end{pmatrix} \tag{2.58}$$

An analogous calculation leads to

$$\epsilon = -\frac{\hbar |v_x|}{W}\left(\pi\left(l - \frac{1}{2}\right) + \arcsin\frac{\epsilon}{|\Delta|} + \frac{\chi}{2}\right) \tag{2.59}$$

The final result for the spectrum is

$$\epsilon = \pm\frac{\hbar |v_x|}{W}\left(\pi\left(l \pm \frac{1}{2}\right) \mp \arcsin\frac{\epsilon}{|\Delta|} + \frac{\chi}{2}\right) \tag{2.60}$$

The upper sign is equivalent to $k_x > 0$ and the lower sign is equivalent to $k_x < 0$.
Normalizing the wave functions yields the coefficient

$$|A|^2 = \frac{1}{2(W + k_S^{-1})} = \frac{1}{2}\frac{\sqrt{|\Delta|^2 - \epsilon^2}}{\hbar|v_x| + W\sqrt{|\Delta|^2 - \epsilon^2}}. \tag{2.61}$$

Limit of short junction

For junctions with small width W,

$$W \ll \frac{\hbar v_x}{|\Delta|}, \quad \xi \ll W \tag{2.62}$$

where $\xi \sim \hbar v_F/|\Delta|$ is the coherence length. Then, in eq. (2.53) the term with $e^{2ik_nW} \approx 1$ and the spectrum becomes

$$\epsilon = \mp \cos\frac{\chi}{2}, \quad 0 < \chi < \pi \tag{2.63}$$

Limit of long junction

Long junction, $W \gg \xi_0$, it hold that

$$W \gg \frac{\hbar|v_x|}{|\Delta|} \tag{2.64}$$

then the spectrum is (because $\arcsin\frac{\epsilon}{|\Delta|}$ can be neglected

$$\epsilon = \pm\frac{\hbar|v_x|}{W}\left(\frac{\chi}{2} - \frac{\pi}{2}\right) + \frac{l\pi\hbar|v_x|}{W} \tag{2.65}$$

2.4 Supercurrent through the SNS junction

Having established the normal wave functions for SNS junctions, the quantum-mechanical current can be calculated.

$$\mathbf{j} = \frac{e}{m}\left[f_n u_n^*(\mathbf{r})\left(-i\hbar\nabla - \frac{e}{c}\mathbf{A}\right)u_n(\mathbf{r}) + \left(1 - f_n\right)v_n(\mathbf{r})\left(-i\hbar\nabla - \frac{e}{c}\mathbf{A}\right)v_n^*(\mathbf{r}) + \text{c.c.}\right] \tag{2.66}$$

n labels quantum states, f_n is the corresponding Fermi distribution. As a simplification, $\mathbf{A} = 0$ is considered. For evaluating eq. (2.66), the normal wave functions from eq. (2.46) are used. In the semi-classical approximation, only the derivatives of the rapidly varying functions $e^{i\mathbf{kr}}$ contribute to the current.

$$\mathbf{j} = -i\hbar\frac{e}{m}\left[f_n u_n^*(\mathbf{r})\nabla u_n(\mathbf{r}) + \left(1 - f_n\right)v_n(\mathbf{r})\nabla v_n^*(\mathbf{r}) + \text{c.c.}\right] \tag{2.67}$$

$$I_x = -\frac{e}{\hbar}\sum_n \left(1 - 2f_n\right)\frac{\hbar v_x\sqrt{|\Delta^2| - \epsilon_n^2}}{\hbar v_x + W\sqrt{|\Delta|^2 - \epsilon^2}} \tag{2.68}$$

2.5 Specular Andreev reflection, graphene specifics

An unusual form of Andreev reflection has been found on graphene - superconductor interfaces [2]. The previously discussed Andreev reflection changes the direction of the incoming particle so that the reflected particle travels on the same trajectory as the incoming one. This process is called

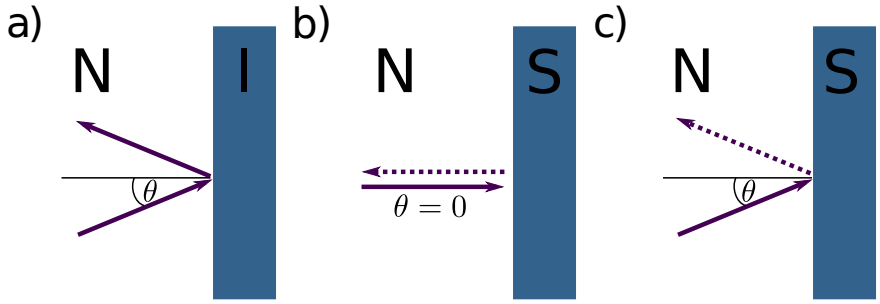

Figure 2.4: *Reflection processes. Solid arrows represent electrons, dashed arrows represent holes.*
a) Specular reflection of an electron at an insulating interface (I).
b) Andreev retro reflection of an electron with into a hole.
c) Specular Andreev reflection of an electron into an hole with incident angle $\theta \neq 0$.

Andreev retro reflection and is illustrated in figure 2.4 b. It is only an approximation, because due to its condensation into a cooper pair, the particle will lose energy during the reflection process. In most metals, hardly any energy loss is observed because the Fermi energy of most metals is large compared to the superconducting energy gap, $E_F \gg \Delta$ [3]. Graphene, however, is a semi-metal with low E_F, where the regime with $E_F < \Delta$ is achievable. As a consequence, E_F dependence of Andreev reflection can be studied in graphene.
The single particle Hamiltonian for graphene is the Dirac Hamiltonian

$$H = \begin{pmatrix} H_+ & 0 \\ 0 & H_- \end{pmatrix} \tag{2.69}$$

$$H_\pm = i\hbar\left(\sigma_x\delta_x \pm \sigma_y\delta_y\right) + U \tag{2.70}$$

This modifies the BdG-equation to

$$\begin{pmatrix} H_\pm + E_F & \Delta \\ \Delta^* & E_F - H_\pm \end{pmatrix}\begin{pmatrix} u \\ v \end{pmatrix} = \epsilon\begin{pmatrix} u \\ v \end{pmatrix}, \tag{2.71}$$

where the electron spinor has two components $\left(u_1, u_2\right) = \left(\Psi_{A+}, \Psi_{B+}\right)$, and the hole spinor is $\left(v_1, v_2\right) = \left(\Psi^*_{A-} - \Psi^*_{B-}\right)$. Eq. (2.71) leads to the energy spectrum

$$\epsilon = \sqrt{|\Delta|^2 + \left(E_F - U \pm \hbar v|\mathbf{k}|\right)^2}, \tag{2.72}$$

with

$$|\mathbf{k}| = \sqrt{k_x^2 + k_y^2}. \tag{2.73}$$

The dispersion relation has four solutions for $\mathbf{k}$. Two of them lead to a positive velocity $v_x = \hbar^{-1} d\epsilon dk_x$ corresponding to each one electronic and one hole excitation. A reflected hole can be in one of the following two states: It is reflected either into the conduction band with $\epsilon < E_F$ (retro reflection) or into the valence band with $\epsilon > E_F$ (specular reflection). Specular reflection is the dominating process, when the Fermi energy is smaller than the gap energy, $E_F \ll \Delta$. For $E_F \gg \Delta$, the retro reflection dominates.

3 Analytical Model

3.1 Foundation of the quasiclassical model

From section 2.3 it is known that Andreev reflection of electrons in a SNS junction leads to Andreev bound states within the junction. Each one of these bound states contributes to the total current through the junction. Essentially, a bound state can be expressed as a trajectory from one superconductor through the normal metal to the other superconductor. The superconducting current density is found through geometrical analysis of possible trajectories. The total current density is then found by adding up all these trajectories. The two dimensional junction (schematic

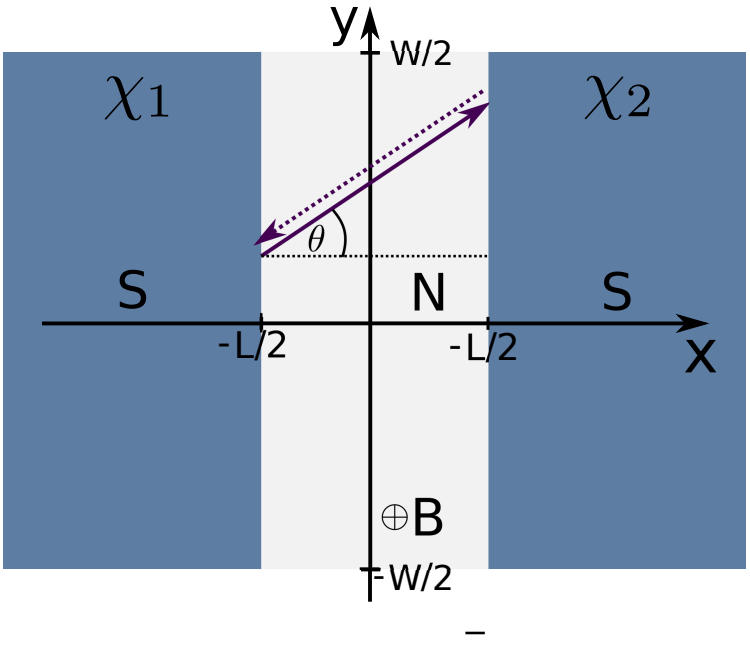

Figure 3.1: *Schematic representation of a short and wide SNS junction.*

shown in fig 3.1) is a short and wide junction with width W and length L, where $W \gg L$. The NS-interfaces are parallel to the y-axis and are placed at $x = \pm L/2$. Each of the superconducting leads has a phase χ_1 and χ_2, and the overall phase difference is $\chi = \chi_1 - \chi_2$. The superconducting gap parameter Δ is only present in the superconducting leads. Close to the interface, Δ begins to decay on a length scale of the superconducting coherence length ξ_0 into the normal region. Similar to the procedure in section 2.3, this decay is neglected and a step-like behaviour is assumed for

the superconducting gap parameter:

$$\Delta(x) = |\Delta| e^{\chi_1} \Theta\left(-L/2 - x\right) + |\Delta| e^{\chi_2} \Theta\left(x - L/2\right). \tag{3.1}$$

The thermal length scale of the system assumed to be larger than the sample length:

$$L_T = \hbar v_F / k_B T \gg L. \tag{3.2}$$

The transport through the junction is assumed to be ballistic, resulting in the trajectories being straight and not being altered by scattering in the normal region. However, the presence of the magnetic field in the normal region of the sample will lead to a bending of the trajectories due to the Lorentz force. Depending on the strength of magnetic field B and the Fermi velocity, the radius of this curve is

$$r_B = \frac{m v_F}{eB} \tag{3.3}$$

In order to justify the assumption of straight trajectories, either the magnetic field has to be weak enough, or the Fermi velocity (wavelength) has to be large (short) enough. Then, the cyclotron radius r_B is larger than the sample size L, and straight trajectories are a valid assumption.

3.2 Plane setup: calculation of current

Summing up the contributions leads to the current through the SNS junctions, the Josephson current $J(\chi)$, which is a function of the superconducting phase difference $\chi = \chi_2 - \chi_1$. By maximizing the Josephson current with respect to χ, one finds the critical current I_c.
A trajectory connecting the two superconducting interfaces can be parametrized by the angle θ between the trajectory and the x-axis. For a trajectory from a point $(-L/2, y_1)$ to another at $(+L/2, y_2)$, the angle for the parametrization is

$$\tan\theta = \frac{y_2 - y_1}{L}. \tag{3.4}$$

Figure 3.1 visualizes this parametrization. Several papers outline approaches to this problem ([4], [5]) and are based on the same concept. The Josephson current in [4] has the form

$$J = \frac{2e}{\pi L} \sum_{\boldsymbol{\kappa}} v_{Fx}^{\boldsymbol{\kappa}} \mathcal{J}(\chi), \tag{3.5}$$

where $\boldsymbol{\kappa}$ is the tangential momentum with $\boldsymbol{\kappa}^2 + \mathbf{k_x}^2 = k_F^2$. v_{Fx} is the projection of v_F on the x-axis

$$v_{Fx} = v_F \cos\theta \tag{3.6}$$

and $\mathcal{J}(\chi)$ is the current density. A similar ansatz to eq. (3.5) is described in [6]:

$$J = \int_{-W/2}^{+W/2} dy \int_{-p_F}^{+p_F} \frac{dp_y}{2\pi} \cos\theta \mathcal{J}(\chi, \phi). \tag{3.7}$$

For a fixed point at the left interface, the current density is integrated over all possible momenta. This integral can be expressed through the endpoints of a trajectory. The integration over p_y can then be replaced by $p_y = p_F \sin\theta \rightarrow dp_y/d\theta = p_F \cos\theta$. The integration over the angle θ can be substituted by the integration over y_2, a point at the right interface. The result for the Josephson current reads

$$J(\chi, \phi = 0) = \frac{2e v_F}{\pi \lambda_F L^2} \int \int_{-W/2}^{W/2} dy_1 dy_2 \frac{\mathcal{J}(\chi)}{\left[1 + \left(\frac{y_1 - y_2}{L}\right)^2\right]^2}. \tag{3.8}$$

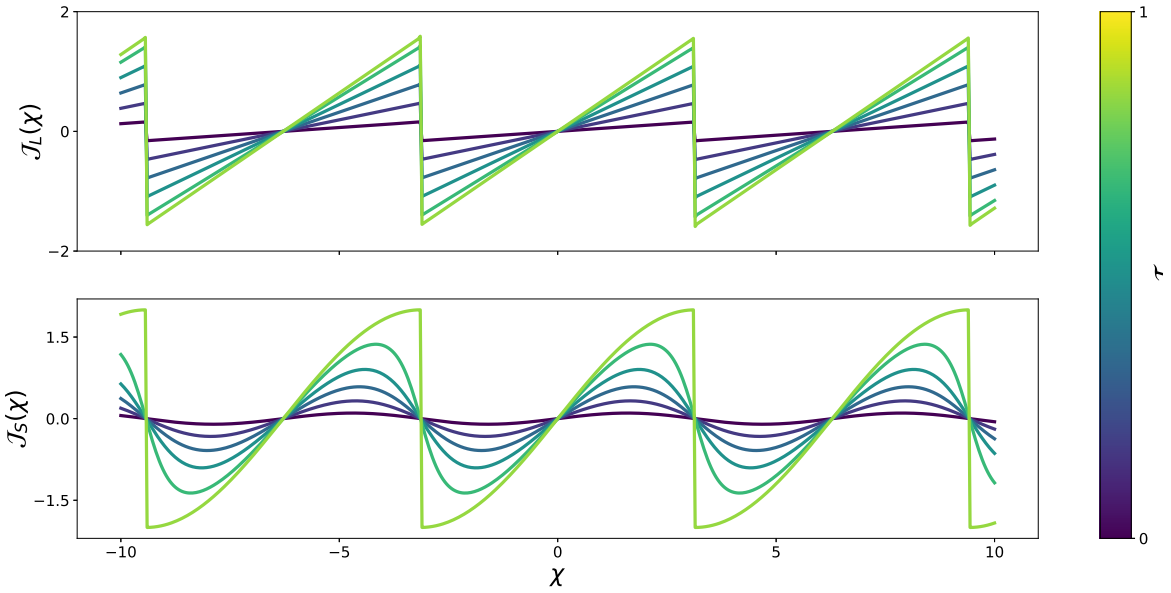

Figure 3.2: *Short and long junction current density*

By maximizing the Josephson current with respect to χ, the critical current can be found as:

$$I_c(\phi) = \max_\chi \left\{ J(\chi, \phi) \right\}. \tag{3.9}$$

The current density $\mathcal{J}$ depends on the ratio of W and L. For $W \gg L$, the junction is a short junction, while for $W \ll L$, it is a long junction. In the short junction limit, the current density is calculated in [7]

$$\mathcal{J}^s(\chi) = \frac{\mathcal{T}_n \sin\chi}{\sqrt{1 - \mathcal{T}_n \sin^2 \frac{\chi}{2}}} \tag{3.10}$$

which can be derived in the framework of the scattering matrix formalism. $\mathcal{T}_n$ is the transmission coefficient for a given conducting channel. For low transmission, $\mathcal{T} \ll 1$, only the first addend contributes, which leads to the conventional Josephson relation $J \simeq \mathcal{T} \sin\chi$.
For the long junction, from [5] the following expression can be found:

$$\mathcal{J}^l(\chi) = \sum_{k=1}^{\infty} \frac{(-1)^{k+1}}{k} \sin\big(k\chi\big). \tag{3.11}$$

The coefficient $\mathcal{T}$ has been included phenomenologically in this formula and includes the normal scattering in the sample. Figure 3.2 shows a plot of both short and long junction limit current densities. For $\mathcal{T} \ll 1$, $\mathcal{J}^s$ takes a sinusoidal form, which also true for the long junction limit. For each of those, the classical Josephson relation can be found in the limit of low transmissions. The current densities differ for a large transmission coefficient $\mathcal{T} \simeq 1$: A sawtooth-like shape is observed in the long junction limit, and in the short junction limit, a sinusoidal shape appears.

Including magnetic field

Up to this point, the current has been derived for zero magnetic field. If a finite magnetic field is considered, the phase χ is modified because of two effects: First, the magnetic phase that will be acquired along a trajectory connecting two points y_1 and y_2 leads to an additional term in the phase. Also, the superconducting phases at each interface become functions of $y_{1/2}$ (see [6]):

$$\chi_{1/2} = \mp\frac{1}{2}\left(\chi - \frac{2\pi BL}{\phi_0}y_{1/2}\right) \tag{3.12}$$

$$\tilde{\chi}(y_1, y_2) = \chi_2 - \chi_1 \tag{3.13}$$

$$= \chi - \frac{\pi BL}{\phi_0}(y_1 + y_2) \tag{3.14}$$

Assuming that the London penetration depth is small to zero in the superconducting regions, the following gauge for the vector potential can be used:

$$\mathbf{A} = A_y\mathbf{e}_y, \quad A_y = \begin{cases} -Bx, & -L/2 \le x \le L/2, \\ -\frac{1}{2}BL|x|, & |x| > L/2 \end{cases} \tag{3.15}$$

This gauge will give no additional contribution to the phase on straight trajectories

$$\delta\chi = \frac{2\pi}{\Phi_0}\int d\mathbf{l}\cdot\mathbf{A} \tag{3.16}$$

$$= \frac{2\pi}{\Phi_0}\int_{-L/2}^{L/2}\frac{dx}{\cos\theta}A_y(x)\sin\theta \tag{3.17}$$

$$= -\frac{2\pi B}{\Phi_0}\frac{y_2 - y_1}{L}\int_{-L/2}^{L/2}x dx \tag{3.18}$$

$$= 0, \tag{3.19}$$

where eq. (3.4) has been used. The total phase for this setup is therefore eq. (3.14). This results in the current phase relation in the expression for the Josephson current from eq. (3.8) to be replaced by the effective phase $\chi \to \tilde{\chi}(y_1, y_2)$:

$$J\left(\chi, \phi\right) = \frac{2ev_F}{\pi\lambda_F L^2}\int\int_{-W/2}^{W/2}dy_1 dy_2 \frac{\mathcal{J}(\tilde{\chi}(y_1, y_2))}{\left[1 + \left(\frac{y_1 - y_2}{L}\right)^2\right]^2} \tag{3.20}$$

By maximizing the Josephson current with respect to χ, the critical current can be found as:

$$I_c(\phi) = \max_\chi\left\{J(\chi, \phi)\right\} \tag{3.21}$$

3.3 Calculation of QPC current

The quasi classical formalism can even be employed to modified SNS junctions. One can build gates on top of the normal region of the junction in a way that the current cannot pass through the gated regions (see chapter 1). In the quasi classical picture, this means that the possibilities for trajectories connecting two points at the superconducting interfaces are limited through the geometry of the constriction.
Figure 3.3 shows a sketch of the quantum point contact set-up which will be analysed with the

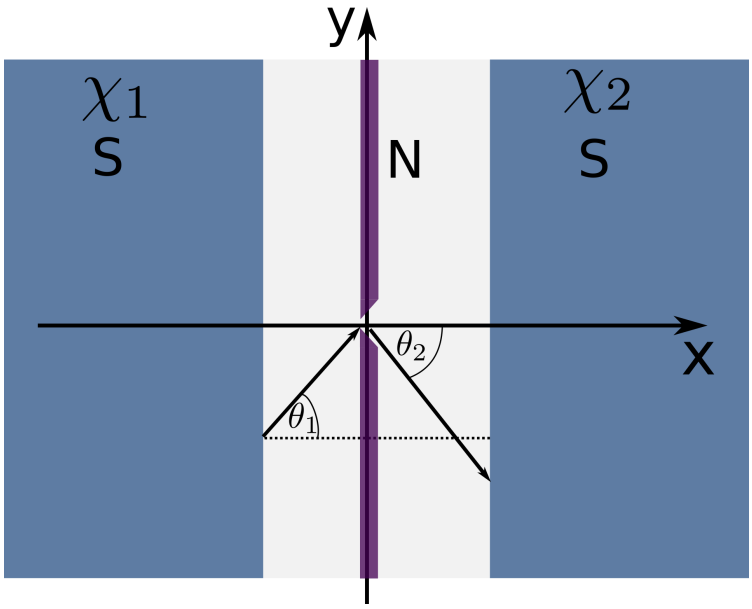

Figure 3.3: *QPC setup.*

quasi classical formalism. The normal region of the SNS junction is covered by a gate with a small split in the middle. The split is located at $(x, y) = (0, 0)$ so that the sample is symmetric around the origin. The width of the split is in the order of λ_F and can thereby be viewed as an isotropic scattering point with transmission coefficient $\mathcal{T}_0$. Trajectories connecting the two superconducting interfaces have to pass through the QPC. For simplicity, the geometrical width of the barrier is neglected, only straight trajectories are considered, and scattering at side edges is neglected. This modified set-up leads to a different parametrization of the trajectories and therefore to a different magnetic phase than in eq. (3.14).
With the QPC set-up, all possible trajectories are parametrized by two angles θ_1 and θ_2. θ_1 describes the trajectory before passing through the QPC in the region $-L/2 < x < 0$, and θ_2 after passing through the QPC. The parametrization of the trajectories reads

$$\tan\theta_1 = -\frac{2y_1}{L}, \quad \tan\theta_2 = \frac{2y_2}{L} \tag{3.22}$$

With the gauge from eq. (3.15), the magnetic phase acquired within the sample reads

$$\frac{2\pi}{\Phi_0}\int d\mathbf{l}\cdot\mathbf{A} \;=\; -\frac{\pi B}{\Phi_0}\left(\frac{L}{2}\right)^2\left(-\tan\theta_1+\tan\theta_2\right) = -\frac{\pi\phi(y_1+y_2)}{2W}. \tag{3.23}$$

Adding this contribution to the term in eq. (3.14), the effective phase for the QPC setup is found to be

$$\tilde{\chi}(y_1, y_2) = \chi - \frac{3\pi\phi}{2W}(y_1 + y_2). \tag{3.24}$$

One consequence of the additional gate on top of the normal region is the change in the effective phase, resulting in a modified current phase relation $\mathcal{J}(\tilde{\chi}(y_1, y_2))$. Another consequence is a modified expression for the critical current. In the set-up without gates, straight trajectories with a fixed angle θ were considered and summed up to a total contribution. The difference in the QPC set-up is the split in the gate, which is modelled as an isotropic scattering point. The trajectories being summed up in this set-up can be thought to consist of two parts. The first part connects y_1 with the split at $(x, y) = (0, 0)$ and is determined by the direction of the trajectory. This explains

the Fermi velocity in this part(?). The second part of the current trajectory starts from the origin and connects it with a point at the right interface y_2. Summing up, the critical current in the QPC set-up is

$$I_c^{\mathrm{QPC}}(\phi) \propto \max_\chi \int d\theta_1 v_F \cos^2\theta_1 \int d\theta_f \cos\theta_f \mathcal{J}\left(\tilde{\chi}(\theta_1,\theta_2)\right) \tag{3.25}$$

The QPC is modelled as an isotropic scatterer with transmission probability $\mathcal{T}$. If the transmission is small, $\mathcal{T} << 1$, eq. (3.9) can be used for $\mathcal{J}$. The angles $\theta_{1,2}$ can be rewritten in terms of $y_{1,2}$ by using the parametrization from eq. (3.22), allowing the normalized critical current to be expressed as

$$\frac{I_c(\phi)}{I_c(0)} = \frac{\mathcal{I}_2(\phi)\mathcal{I}_{3/2}(\phi)}{\mathcal{I}_2(0)\mathcal{I}_{3/2}(0)}, \tag{3.26}$$

where the integrals $\mathcal{I}$ are defined as

$$\mathcal{I}_k(\phi) = \frac{2}{L}\int_{-W/2}^{+W/2} dy \frac{\cos\left(\frac{3\pi\phi y}{2W}\right)}{\left[1+\left(\frac{2y}{L}\right)^2\right]^k} \tag{3.27}$$

The current can be evaluated in the limit of small flux $\phi \to 0$, and in limit of high fields $\phi \to \infty$. At $\phi = 0$ the cosine term becomes one leading to the simple expression

$$\mathcal{I}_2(0)\mathcal{I}_{3/2}(0) = \frac{2W}{\sqrt{L^2+W^2}}\arctan\frac{W}{L} + \frac{2LW^2}{(L^2+W^2)^{3/2}} \tag{3.28}$$

$$\equiv \frac{2x}{\sqrt{1+x^2}}\arctan x + \frac{2x^2}{\left(1+x^2\right)^{3/2}}, \quad x = W/L \tag{3.29}$$

The parabolic asymptotics of the critical current at small ϕ is found by expanding the cosine factors in the numerator:

$$\frac{I_c(\phi)}{I_{c0}} \simeq 1 - \frac{9\pi^2\phi^2}{32} f_0(W/L) \tag{3.30}$$

$$f_0(x) = \frac{\sqrt{x^2+1}\log\left(\sqrt{x^2+1}+x\right)}{x^3} - \frac{2}{x(x+(x^2+1)\arctan x)} \tag{3.31}$$

In the opposite limit of high fields, $\phi \to \infty$, the integration in eq. (3.27) is extended over y_1 and y_2 to $\pm\infty$ and obtain

$$\frac{I_c(\phi)}{I_{c0}} = \frac{\pi^2\left(1+x^2\right)^{3/2}}{4x\left(x+\left(1+x^2\right)\arctan x\right)}\left(1+\frac{3\pi\phi}{4x}\right)\sqrt{\frac{3\phi}{2x}}\exp\left(-\frac{3\phi\pi}{2x}\right) \tag{3.32}$$

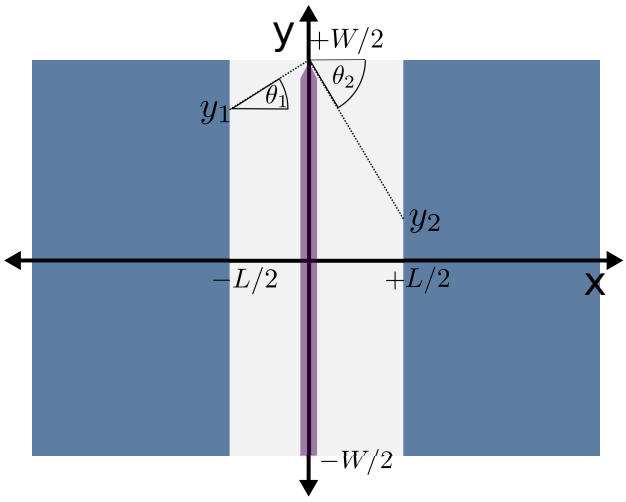

Figure 3.4: *A figure caption.*

3.4 QPC edge current

Additionally to the QPC, two edge channels at $(x, y) = (0, \pm w/2)$ are introduced. The QPC is modelled with the transmission coefficient $\mathcal{T}_q$, and the edge channel with the coefficient $\mathcal{T}_e$. The lattice orientation of the graphene structure may may be either predominantly arm-chair or zigzag. Depending on this orientation, the edge currents may or may not contribute significantly to the total current. The Fraunhofer pattern changes accordingly.

The parametrization of an edge trajectory, illustrated in figure **??**, reads

$$\tan\theta_1 = \frac{W - y_1}{L/2}, \quad \tan\theta_2 = -\frac{W - y_2}{L/2}. \tag{3.33}$$

Similar to the QPC contribution, the magnetic phase gain along the trajectory is calculated. For the upper edge, the result is

$$\begin{aligned}
\frac{2\pi}{\phi_0}\int d\mathbf{l}\cdot\mathbf{A} &= \frac{2\pi}{\phi_0}\left(\int A_y(x)|d\mathbf{l}||\mathbf{e_y}|\sin\theta_1 + \int A_y(x)|d\mathbf{l}||\mathbf{e_y}|\sin\theta_2\right) && (3.34)\\
&= -\frac{2\pi B}{\phi_0}\left(\int_{-L/2}^{0} x dx\tan\theta_1 + \int_0^{L/2} x dx\tan\theta_2\right) && (3.35)\\
&= -\frac{\pi B}{\phi_0}\frac{L}{2}\left(-\tan\theta_1 + \tan\theta_2\right) && (3.36)\\
&= -\frac{\pi B}{\phi_0}\frac{L}{2}\left(-2W + (y_1 + y_2)\right) && (3.37)\\
&= \pi\Phi - \frac{\pi\Phi}{2W}(y_1 + y_2), && (3.38)
\end{aligned}$$

where

$$\Phi = \frac{\phi}{\phi_0}, \quad \phi = BWL \tag{3.39}$$

has been used. Together with the contribution from the set-up without any constriction from eq. (3.14), the total phase for the edge transmission is added up to

$$\tilde{\chi}(y_1, y_2) = \chi - \frac{3\pi\Phi}{2\phi_0}(y_1 + y_2) + \pi\Phi. \tag{3.40}$$

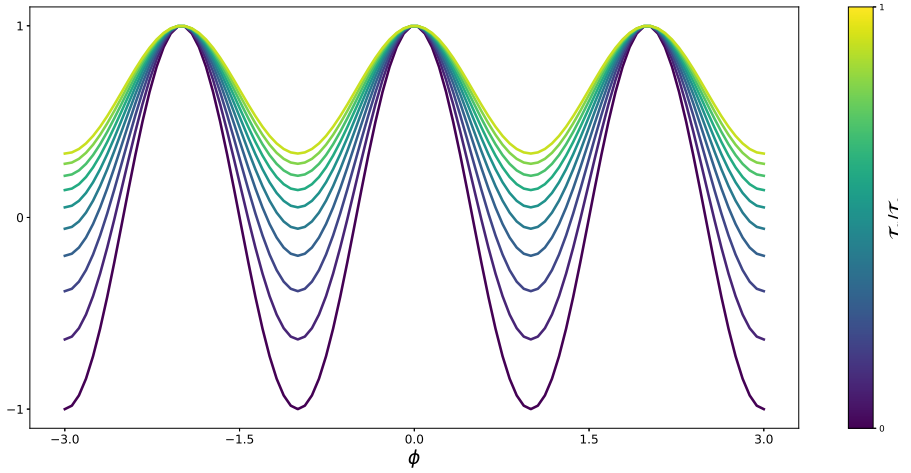

This is the effective phase $\tilde{\chi}(y_1, y_2)$ for the upper edge. Analogously, the phase for the lower edge can be constructed with a simple sign change in the parametrization in eq. (3.33), leading to

$$\tilde{\chi}(y_1, y_2) = \chi + \frac{3\pi\Phi}{2\phi_0}(y_1 + y_2) - \pi\Phi \tag{3.41}$$

The Josephson relation for the edge contribution has the modified phase from eq. (3.41). The result for the QPC in the limit in high fields, eq. (3.32), has a transmission coefficient $\mathcal{T} = 1$. For easier comparison with the edge channel contribution, this is rewritten into the following form

$$I_c^{\mathrm{QPC}} = \mathcal{T}_q F(W/L) \tag{3.42}$$

The integrals for the upper edge current at high fields look very similar to the QPC result.

$$I_c^e = \mathcal{T}_e \sin\left(\chi_0 - \pi\Phi\right) \int_0^\infty d\tilde{y}_1 \int_0^\infty d\tilde{y}_2 \frac{\cos\left(\frac{3\pi\Phi\tilde{y}_1}{2W}\right)}{\left(1 + \left(\frac{2\tilde{y}_1}{L}\right)^2\right)^2} \frac{\cos\left(\frac{3\pi\Phi\tilde{y}_2}{2W}\right)}{\left(1 + \left(\frac{2\tilde{y}_1}{L}\right)^2\right)^{3/2}} \tag{3.43}$$

$$= \mathcal{T}_e \sin\left(\chi_0 - \pi\Phi\right) \frac{F(W/L)}{4}, \tag{3.44}$$

where

$$\tilde{y}_{1/2} = W/2 - y_{1/2} \tag{3.45}$$

The total critical current though the junction is proportional to the sum of the individual contributions

$$\frac{I_c\left(\phi\right)}{I_{c0}} = \max_\chi \left\{ \mathcal{T}_q \sin\chi + \frac{\mathcal{T}_e}{4} \sin\left(\chi - \pi\phi\right) + \frac{\mathcal{T}_e}{4} \sin\left(\chi + \pi\phi\right) \right\} / \left(\mathcal{T}_q + \mathcal{T}_e/2\right) \tag{3.46}$$

$$= \frac{\mathcal{T}_q/\mathcal{T}_e + \cos\left(\pi\phi\right)/2}{\mathcal{T}_q/\mathcal{T}_e + 1/2} \tag{3.47}$$

The result of eq. (3.47) is plotted in figure **??**.

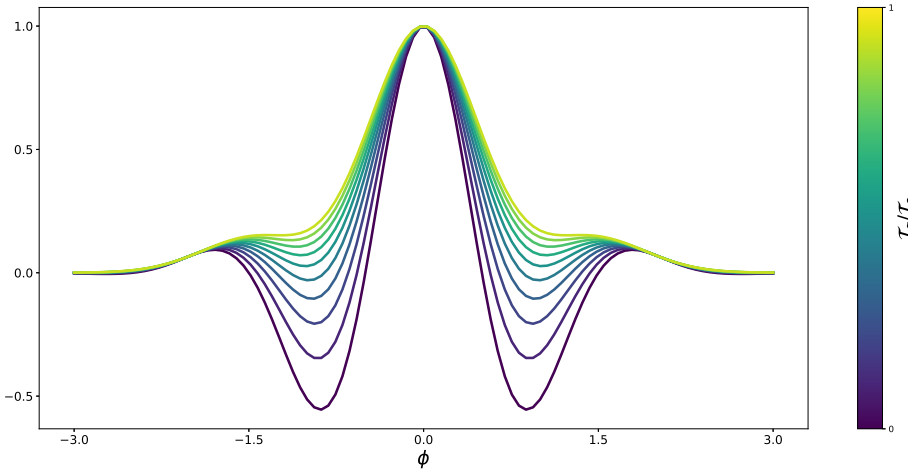
1.0
0.5
0.0
−0.5
−3.0
−1.5
0.0
1.5
3.0
ϕ
1
0
τ_-/τ_-

Bibliography

[1] J. Bardeen, L. N. Cooper and J. R. Schrieffer. Theory of Superconductivity. *Physical Review*, 108(5):1175–1204, dec 1957.

[2] C. W. J. Beenakker. Specular Andreev reflection in graphene. apr 2006.

[3] Dmitri K. Efetov and Konstantin B. Efetov. Crossover from retro to specular Andreev reflections in bilayer graphene. *Physical Review B*, 94(7), 2016.

[4] Alexandre M. Zagoskin. The half-periodic Josephson effect in an s-wave superconductor-normal-metal-d-wave superconductor junction. *Journal of Physics Condensed Matter*, 9(31), 1997.

[5] Victor Barzykin and Alexandre M. Zagoskin. Coherent transport and nonlocality in mesoscopic SNS junctions: Anomalous magnetic interference patterns. *Superlattices and Microstructures*, 25(5):797–807, 1999.

[6] Hendrik Meier, Vladimir I. Fal'Ko and Leonid I. Glazman. Edge effects in the magnetic interference pattern of a ballistic SNS junction. *Physical Review B*, 93(18):1–13, 2016.

[7] C. W J Beenakker and H. Van Houten. Josephson current through a superconducting quantum point contact shorter than the coherence length. *Physical Review Letters*, 66(23):3056–3059, 1991.